

HERMITE WENO SCHEMES WITH LAX-WENDROFF TYPE TIME DISCRETIZATIONS FOR HAMILTON-JACOBI EQUATIONS ^{*1)}

Jianxian Qiu

(Department of Mathematics, Nanjing University, Nanjing 210093, China

Email: jxqiu@nju.edu.cn)

Abstract

In this paper, we use Hermite weighted essentially non-oscillatory (HWENO) schemes with a Lax-Wendroff time discretization procedure, termed HWENO-LW schemes, to solve Hamilton-Jacobi equations. The idea of the reconstruction in the HWENO schemes comes from the original WENO schemes, however both the function and its first derivative values are evolved in time and are used in the reconstruction. One major advantage of HWENO schemes is its compactness in the reconstruction. We explore the possibility in avoiding the nonlinear weights for part of the procedure, hence reducing the cost but still maintaining non-oscillatory properties for problems with strong discontinuous derivative. As a result, comparing with HWENO with Runge-Kutta time discretizations schemes (HWENO-RK) of Qiu and Shu [19] for Hamilton-Jacobi equations, the major advantages of HWENO-LW schemes are their saving of computational cost and their compactness in the reconstruction. Extensive numerical experiments are performed to illustrate the capability of the method.

Mathematics subject classification: 65M06, 65M99, 70H20.

Key words: WENO scheme, Hermite interpolation, Hamilton-Jacobi equation, Lax-Wendroff type time discretization, High order accuracy.

1. Introduction

In this paper, we study an alternative method for time discretization, namely the Lax-Wendroff type time discretization [11], to the popular TVD Runge-Kutta time discretization in [21], for Hermite weighted essentially non-oscillatory (HWENO) schemes [17, 18, 19], termed HWENO-LW schemes, for solving the Hamilton-Jacobi (HJ) equations

$$\begin{cases} \phi_t + H(\nabla_x \phi) = 0, \\ \phi(x, 0) = \phi_0(x), \end{cases} \quad (1.1)$$

where $x = (x_1, \dots, x_d)$ are d -spatial variables. The HJ equations appear often in applications, such as in control theory, differential games, geometric optics and image processing. The solutions to (1.1) typically are continuous but with discontinuous derivatives, even if the initial condition $\phi_0(x) \in C^\infty$. It is well known that the HJ equations are closely related to conservation laws, hence successful numerical methods for conservation laws can be adapted for solving the HJ equations. Along this line we mention the early work of Osher and Sethian [13] and Osher and Shu [14] in constructing high order ENO (essentially non-oscillatory) schemes for solving the HJ equations. Central high resolution schemes were developed in [2, 10]. Finite element methods suitable for arbitrary triangulations were developed in [1, 3, 6]. The WENO

* Received May 11, 2006; accepted August 31, 2006.

¹⁾ Research partially supported by NNSFC grant 10371118, SRF for ROCS, SEM and Nanjing University Talent Development Foundation.

schemes for solving the HJ equations were constructed in [8] by Jiang and Peng, based on the WENO schemes for solving conservation laws [12, 9, 23], and further Zhang and Shu [24] developed high order WENO schemes on unstructured meshes for solving two-dimensional HJ equations. Finally, most relevant to our work, we mention the HWENO schemes for solving the HJ equations by Qiu and Shu [19], based on the HWENO schemes for solving conservation laws [17, 18].

WENO or HWENO is a spatial discretization procedure, namely, it is a procedure to approximate the spatial derivative terms in (1.1). The time derivative term there must also be discretized. There are mainly two different approaches to approximate the time derivative. The first approach is to use an ODE solver, such as a Runge-Kutta or a multi-step method, to solve the method of lines ODE obtained after spatial discretization. The second approach is a Lax-Wendroff type time discretization procedure, which is also called the Taylor type referring to a Taylor expansion in time or the Cauchy-Kowalewski type referring to the similar Cauchy-Kowalewski procedure in PDE. This approach is based on the idea of the classical Lax-Wendroff scheme [11], and it relies on converting all the time derivatives in a temporal Taylor expansion into spatial derivatives by repeatedly using the PDE and its differentiated versions. The spatial derivatives are then discretized by, e.g. the HWENO approximations.

The Lax-Wendroff type time discretization, usually produces the same high order accuracy with a smaller effective stencil than that of the first approach, and it uses more extensively the original PDE. The original finite volume ENO schemes in [5] used this approach for the time discretization. More recently, a Lax-Wendroff type time discretization procedure for high order finite difference WENO schemes was developed by Qiu and Shu [15]. This approach was also used by Titarev and Toro [22] and Schwartzkopff, et al. [20], termed ADER (arbitrary high order schemes utilizing higher order derivatives), to construct a class of high order schemes for conservation laws in finite volume version. The Lax-Wendroff type time discretization was also used in the discontinuous Galerkin method [4, 16].

In this paper, based on the WENO-LW methodology for conservation laws in [15] and HWENO schemes for HJ equation in [19], we develop HWENO-LW schemes to solve the HJ equations. Comparing with the HWENO-RK schemes of Qiu and Shu [19], the major advantages of HWENO-LW schemes are their saving of computational cost and their compactness in the reconstruction.

The organization of this paper is as follows. In Section 2, we describe in detail the construction and implementation of the HWENO-LW schemes, for one and two-dimensional HJ equations (1.1). In Section 3 we provide extensive numerical examples to demonstrate the behavior of the schemes and to perform a comparison with the HWENO-RK schemes for HJ equations by Qiu and Shu [19]. Concluding remarks are given in Section 4.

2. The Construction of HWENO-LW Schemes for the Hamilton-Jacobi Equations

In this section we will present the details of the construction of HWENO-LW schemes for both one and two-dimensional Hamilton-Jacobi equations.

2.1. One-dimensional Case

We first consider the one dimensional HJ equation (1.1). For simplicity, we assume that the grid points $\{x_{i+1/2}\}$ are uniformly distributed with the cell size $x_{i+1/2} - x_{i-1/2} = \Delta x$ and cell

centers $x_i = \frac{1}{2}(x_{i-1/2} + x_{i+1/2})$. We also denote the cells by $I_i = [x_{i-1/2}, x_{i+1/2}]$. This assumption is not essential: the method can be easily defined for non-uniform meshes.

Letting $u = \phi_x$, and taking the x derivative of (1.1), we obtain the conservation law:

$$\begin{cases} u_t + H(u)_x = 0, \\ u(x, 0) = u_0(x). \end{cases} \quad (2.1)$$

We denote $\phi_i = \phi(x_i, t)$ and the cell averages of u as $\bar{u}_i = \frac{1}{\Delta x} \int_{I_i} u(x, t) dx$, and denote $\phi^{(r)}$ and $u^{(r)}$ by the r -th order time derivative of ϕ and u , respectively. We also use ϕ', ϕ'', ϕ''' and u', u'', u''' to denote the first three time derivatives of ϕ and u , respectively. By a temporal Taylor expansion we obtain

$$\phi(x, t + \Delta t) = \phi(x, t) + \Delta t \phi' + \frac{\Delta t^2}{2} \phi'' + \frac{\Delta t^3}{6} \phi''' + \frac{\Delta t^4}{24} \phi^{(4)} + \dots, \quad (2.2)$$

$$u(x, t + \Delta t) = u(x, t) + \Delta t u' + \frac{\Delta t^2}{2} u'' + \frac{\Delta t^3}{6} u''' + \frac{\Delta t^4}{24} u^{(4)} + \dots \quad (2.3)$$

If we would like to obtain k -th order accuracy in time, we would need to approximate the first k time derivatives: $\phi', \dots, \phi^{(k)}$ and $u', \dots, u^{(k)}$. Although the procedure can be naturally extended to any higher orders, we will proceed up to fourth order in time in this paper, and obtain:

$$\phi_i^{n+1} = \phi_i + \Delta t \phi'_i + \frac{\Delta t^2}{2} \phi''_i + \frac{\Delta t^3}{6} \phi'''_i + \frac{\Delta t^4}{24} \phi_i^{(4)}, \quad (2.4)$$

$$\bar{u}_i^{n+1} = \bar{u}_i + \Delta t \bar{u}'_i + \frac{\Delta t^2}{2} \bar{u}''_i + \frac{\Delta t^3}{6} \bar{u}'''_i + \frac{\Delta t^4}{24} \bar{u}_i^{(4)}, \quad (2.5)$$

where

$$\phi' = -H(u), \quad \phi'' = -H'(u) \phi'_x, \quad (2.6)$$

$$\phi''' = -H''(u) (\phi'_x)^2 - H'(u) \phi''_x, \quad (2.7)$$

$$\phi^{(4)} = -H'''(u) (\phi'_x)^3 - 3H''(u) (\phi'_x) \phi''_x - H'(u) \phi'''_x, \quad (2.8)$$

and

$$\bar{u}_i^{(l)} = \frac{1}{\Delta x} (\phi_{i+1/2}^{(l)} - \phi_{i-1/2}^{(l)}), \quad l = 1, 2, 3, 4. \quad (2.9)$$

After extensive numerical tests, we have found the following Lax-Wendroff procedure which produces the best balance between cost reduction and ensuring essentially non-oscillatory properties to reconstruct $\phi_x, \phi'_x, \phi''_x, \phi'''_x$, and $\phi', \phi'', \phi''', \phi^{(4)}$.

Step 1. The reconstruction of the first time derivative $\phi' = -H(u)$.

We approximate $\phi'_i = -H(u)_i$ and $\phi'_{i+1/2} = -H(u)_{i+1/2}$ by the following schemes

$$\phi'_i = -\tilde{H}_i, \quad \phi'_{i+1/2} = -\hat{H}_{i+1/2}, \quad (2.10)$$

where the numerical fluxes \tilde{H}_i and $\hat{H}_{i+1/2}$ in (2.10) are subject to the usual conditions for numerical fluxes, such as monotonicity, Lipschitz continuity and consistency with the physical flux $H(u)$. For choices of numerical fluxes suitable for the HJ equations we refer to, e.g. [14]. In this paper we use the simple Lax-Friedrichs flux defined by:

$$\tilde{H}_i = H\left(\frac{u_i^- + u_i^+}{2}\right) - \frac{\alpha}{2} (u_i^+ - u_i^-), \quad (2.11)$$

$$\hat{H}_{i+1/2} = \frac{1}{2} \left(H(u_{i+1/2}^-) + H(u_{i+1/2}^+) - \alpha(u_{i+1/2}^+ - u_{i+1/2}^-) \right), \quad (2.12)$$

where u_i^\pm and $u_{i+1/2}^\pm$ are the numerical approximations to the point values of $u(x_i, t)$ and $u(x_{i+1/2}, t)$ respectively from left and right, and $\alpha = \max_u |H'(u)|$. Then the numerical approximations to the point values of $u(x_i, t)$ and $u(x_{i+1/2}, t)$ are taken as $(u_i^+ + u_i^-)/2$ and $(u_{i+1/2}^+ + u_{i+1/2}^-)/2$, respectively. The reconstruction of $\{u_i^\pm\}$ and $\{u_{i+1/2}^\pm\}$ from $\{\phi_i\}$ and $\{\bar{u}_i\}$ is obtained by the fifth order HWENO procedure, for the details we refer to [19], and will not repeat it here.

Step 2. In order to reconstruct the second time derivative $\phi'' = -H'(\phi_x)\phi'_x$, we only need to reconstruct ϕ'_x . The reconstruction of ϕ'_x is obtained as following. Notice that we will only need an approximation of order four, one order lower than before, because of the extra Δt factor. We can use a simple fifth order central difference formulae to approximate the derivative ϕ'_x at the point (x_i, t^n) and $(x_{i+1/2}, t^n)$. We use the following central difference approximation:

$$(\phi'_x)_i \approx \frac{1}{30\Delta x}(9(\phi'_{i-1} - \phi'_{i+1}) + \Delta x(\bar{u}'_{i-1} + 46\bar{u}'_i + \bar{u}'_{i+1})), \quad (2.13)$$

$$(\phi'_x)_{i+1/2} \approx \frac{1}{30\Delta x}(-\phi'_{i-1} - 45\phi'_i + 45\phi'_{i+1} + \phi'_{i+2} - 9\Delta x(u'_i + \bar{u}'_{i+1})). \quad (2.14)$$

Then we get an approximation of ϕ'_i and \bar{u}'_i from (2.6) and (2.9). In fact, we only need an approximation of order four, because of the extra Δt factor, but we would like to use simple central differences which are all of odd order. It seems that a more costly HWENO approximation is *not* needed here to control spurious oscillations, presumably because this term is multiplied by an extra Δt anyway.

Step 3. The third time derivative $\phi''' = -H''(\phi_x)(\phi'_x)^2 - H'(\phi_x)\phi''_x$. Similar to step 2, we only need to reconstruct ϕ''_x . We get the approximation of ϕ''_x by the third order central difference formulae:

$$(\phi''_x)_i \approx \frac{1}{6\Delta x}(\phi''_{i-1} - \phi''_{i+1}) + 8\Delta x\bar{u}''_i, \quad (2.15)$$

$$(\phi''_x)_{i+1/2} \approx \frac{1}{6\Delta x}(-8\phi''_i + 8\phi''_{i+1} - \Delta x(u''_i + \bar{u}''_{i+1})). \quad (2.16)$$

Then, we get an approximation of ϕ''' at the points x_i and $x_{i+1/2}$ from (2.7), and obtain \bar{u}''' on the cell I_i from (2.9). Again, it seems that a more costly HWENO approximation is *not* needed here to control spurious oscillations.

Step 4. The fourth time derivative $\phi^{(4)} = -H'''(\phi_x)(\phi'_x)^3 - 3H''(\phi_x)\phi''_x\phi'_x - H'(\phi_x)\phi'''_x$ is obtained in a similar fashion. We can use the following third order approximation:

$$(\phi'''_x)_i \approx \frac{1}{6\Delta x}(\phi'''_{i-1} - \phi'''_{i+1}) + 8\Delta x\bar{u}'''_i, \quad (2.17)$$

$$(\phi'''_x)_{i+1/2} \approx \frac{1}{6\Delta x}(-8\phi'''_i + 8\phi'''_{i+1} - \Delta x(u'''_i + \bar{u}'''_{i+1})). \quad (2.18)$$

Then, we get an approximation of $\phi^{(4)}$ at the points x_i and $x_{i+1/2}$ from (2.8), and obtain $\bar{u}^{(4)}$ on the cell I_i from (2.9). Again, it seems that a more costly HWENO approximation is *not* needed here to control spurious oscillations.

If we require higher order accuracy in time this procedure can be continued in a similar fashion. The final approximation at the next time step is then given by (2.4) and (2.5).

2.2. Two-dimensional Case

We now proceed to consider the two dimensional HJ equation (1.1). For simplicity of presentation, we again assume that the mesh is uniform with the cell sizes $x_{i+\frac{1}{2}} - x_{i-\frac{1}{2}} = \Delta x$, $y_{j+\frac{1}{2}} - y_{j-\frac{1}{2}} = \Delta y$ and the cell centers $(x_i, y_j) = \left(\frac{1}{2}(x_{i+\frac{1}{2}} + x_{i-\frac{1}{2}}), \frac{1}{2}(y_{j+\frac{1}{2}} + y_{j-\frac{1}{2}})\right)$. This

assumption is again non-essential: the algorithm can be easily defined for tensor product non-uniform meshes. We denote the cells by $I_{ij} = [x_{i-\frac{1}{2}}, x_{i+\frac{1}{2}}] \times [y_{j-\frac{1}{2}}, y_{j+\frac{1}{2}}]$. Let $u = \frac{\partial \phi}{\partial x}$, $v = \frac{\partial \phi}{\partial y}$. Taking the derivatives of (1.1), we obtain

$$\begin{cases} u_t + H_x = 0, \\ u(x, y, 0) = \frac{\partial \phi_0(x, y)}{\partial x}; \end{cases} \quad (2.19)$$

$$\begin{cases} v_t + H_y = 0, \\ v(x, y, 0) = \frac{\partial \phi_0(x, y)}{\partial y}. \end{cases} \quad (2.20)$$

We denote $\phi_{ij}(t) = \phi(x_i, y_j, t)$, and the x cell average of u as $\bar{u}_{ij}(t) = \frac{1}{\Delta x} \int_{x_{i-1/2}}^{x_{i+1/2}} u(x, y_j, t) dx$, the y cell average of v as $\bar{v}_{ij}(t) = \frac{1}{\Delta y} \int_{y_{j-1/2}}^{y_{j+1/2}} v(x_i, y, t) dy$. Similar to the procedure in one dimensional case, we again proceed up to the fourth order in time by a temporal Taylor expansion to obtain

$$\phi_{ij}^{n+1} = \phi_{ij} + \Delta t \phi'_{ij} + \frac{\Delta t^2}{2} \phi''_{ij} + \frac{\Delta t^3}{6} \phi'''_{ij} + \frac{\Delta t^4}{24} \phi^{(4)}_{ij}, \quad (2.21)$$

$$\bar{u}_{ij}^{n+1} = \bar{u}_{ij} + \Delta t \bar{u}'_{ij} + \frac{\Delta t^2}{2} \bar{u}''_{ij} + \frac{\Delta t^3}{6} \bar{u}'''_{ij} + \frac{\Delta t^4}{24} \bar{u}^{(4)}_{ij}, \quad (2.22)$$

$$\bar{v}_{ij}^{n+1} = \bar{v}_{ij} + \Delta t \bar{v}'_{ij} + \frac{\Delta t^2}{2} \bar{v}''_{ij} + \frac{\Delta t^3}{6} \bar{v}'''_{ij} + \frac{\Delta t^4}{24} \bar{v}^{(4)}_{ij}, \quad (2.23)$$

with

$$\phi' = -H, \quad \phi'' = -H_1 \phi'_x - H_2 \phi'_y, \quad (2.24)$$

$$\phi''' = -H_{11} (\phi'_x)^2 - 2H_{12} \phi'_x \phi'_y - H_{22} (\phi'_y)^2 - H_1 \phi''_x - H_2 \phi''_y, \quad (2.25)$$

$$\begin{aligned} \phi^{(4)} = & -H_{111} (\phi'_x)^3 - 3H_{112} (\phi'_x)^2 \phi'_y - 3H_{122} \phi'_x (\phi'_y)^2 - H_{222} (\phi'_y)^3 \\ & - 3H_{11} \phi'_x \phi''_x - 3H_{12} (\phi''_x \phi'_y + \phi'_x \phi''_y) - 3H_{22} \phi'_y \phi''_y - H_1 \phi'''_x - H_2 \phi'''_y, \end{aligned} \quad (2.26)$$

where H_i is the partial derivative of H with respect to i th argument, H_{ij} is the second partial derivative of H with respect to i th and j th arguments and H_{ijk} is the third partial derivative of H with respect to i th, j th and k th arguments, and

$$\bar{u}_{ij}^{(l)} = \frac{1}{\Delta x} (\phi_{i+1/2, j}^{(l)} - \phi_{i-1/2, j}^{(l)}), \quad l = 1, 2, 3, 4, \quad (2.27)$$

$$\bar{v}_{ij}^{(l)} = \frac{1}{\Delta y} (\phi_{i, j+1/2}^{(l)} - \phi_{i, j-1/2}^{(l)}), \quad l = 1, 2, 3, 4. \quad (2.28)$$

Similar to the one dimensional case, what we want to do is to reconstruct $\phi_x, \phi_y, \phi'_x, \phi'_y, \phi''_x, \phi''_y, \phi'''_x, \phi'''_y$ and $\phi', \phi'', \phi''', \phi^{(4)}$ from point values $\{\phi_{ij} = \phi(x_i, y_j, t^n)\}$ and cell averages $\{\bar{u}_{ij}\}$ and $\{\bar{v}_{ij}\}$ respectively.

Similar to Step 1 in the one dimensional case, we approximate $\phi'_{ij} = -H(u)_{ij}$, $\phi'_{i+1/2, j} = -H(u)_{i+1/2, j}$ and $\phi'_{i, j+1/2} = -H(u)_{i, j+1/2}$ by the following Lax-Friedrichs flux:

$$\begin{aligned} \tilde{H}_{ij} &= H\left(\frac{u_{ij}^- + u_{ij}^+}{2}, \frac{v_{ij}^- + v_{ij}^+}{2}\right) - \frac{\alpha_x}{2} (u_{ij}^+ - u_{ij}^-) - \frac{\alpha_y}{2} (v_{ij}^+ - v_{ij}^-), \\ \hat{H}_{i+1/2, j} &= \frac{1}{2} \left(H(u_{i+1/2, j}^-, v_{i+1/2, j}^-) + H(u_{i+1/2, j}^+, v_{i+1/2, j}^+) - \alpha_x (u_{i+1/2, j}^+ - u_{i+1/2, j}^-) \right), \\ \hat{H}_{i, j+1/2} &= \frac{1}{2} \left(H(u_{i, j+1/2}^-, v_{i, j+1/2}^-) + H(u_{i, j+1/2}^+, v_{i, j+1/2}^+) - \alpha_y (v_{i, j+1/2}^+ - v_{i, j+1/2}^-) \right), \end{aligned} \quad (2.29)$$

where u_{ij}^\pm , $u_{i+1/2, j}^\pm$ and $v_{i+1/2, j}^\pm$ are the numerical approximations to the point values of $u(x_i, y_j, t)$, $u(x_{i+1/2}, y_j, t)$ and $v(x_{i+1/2}, y_j, t)$ respectively from left and right, and v_{ij}^\pm , $u_{i, j+1/2}^\pm$ and $v_{i, j+1/2}^\pm$ are the numerical approximations to the point values of $v(x_i, y_j, t)$, $u(x_i, y_{j+1/2}, t)$ and

$v(x_i, y_{j+1/2}, t)$ respectively from bottom and top. The constants α_x and α_y are defined by $\alpha_x = \max_{u,v} |\frac{\partial}{\partial u} H(u, v)|$ and $\alpha_y = \max_{u,v} |\frac{\partial}{\partial v} H(u, v)|$.

The values u_{ij}^\pm , $u_{i+1/2,j}^\pm$, v_{ij}^\pm and $v_{i,j+1/2}^\pm$ can be reconstructed by the one dimensional reconstruction methods presented in the previous subsection with the grid index for the other dimension fixed. The reconstruction procedure of $u_{i,j+1/2}^\pm$ and $v_{i+1/2,j}^\pm$ from $\{\phi_{ij}, \bar{u}_{ij}, \bar{v}_{ij}\}$ can be based either on the fourth order HWENO reconstruction or on the fourth order linear reconstruction, for the details of reconstruction we refer to [19]. In this paper we use the following formula:

$$\begin{aligned} u_{i,j+1/2}^- &= \frac{1}{144} \left\{ \frac{1}{\Delta x} [19(\phi_{i-1,j-1} - \phi_{i+1,j-1}) + 2(\phi_{i-1,j} - \phi_{i+1,j}) - 45(\phi_{i-1,j+1} - \phi_{i+1,j+1})] \right. \\ &\quad + 4(\bar{u}_{i-1,j-1} + \bar{u}_{i+1,j-1} - \bar{u}_{i-1,j} + 30\bar{u}_{ij} - \bar{u}_{i+1,j} - 2\bar{u}_{i-1,j+1} - 2\bar{u}_{i+1,j+1}) \\ &\quad \left. + 6(\bar{v}_{i-1,j-1} - \bar{v}_{i+1,j-1} + \bar{v}_{i-1,j+1} - \bar{v}_{i+1,j+1}) \right\}. \end{aligned} \quad (2.30)$$

The reconstruction for $u_{i,j+1/2}^+$ is mirror symmetric of that for $u_{i,j+1/2}^-$ with respect to $y_{j+1/2}$, and reconstruction for $v_{i+1/2,j}^\pm$ is the same as that for $u_{i,j+1/2}^\pm$ with i and j interchanged.

While HWENO reconstruction is important for the main terms u_{ij}^\pm , $u_{i+1/2,j}^\pm$, v_{ij}^\pm and $v_{i,j+1/2}^\pm$ in each dimension, there is reason to believe that the cross terms $u_{i,j+1/2}^\pm$ and $v_{i+1/2,j}^\pm$ play a lesser role towards spurious oscillations and a linear reconstruction for those terms might be enough. This is indeed verified by our extensive numerical experiments in next section.

After the u^\pm and v^\pm are obtained by the HWENO reconstruction procedure, we get an approximation of ϕ_x and ϕ_y by $\phi_x \approx (u^+ + u^-)/2$ and $\phi_y \approx (v^+ + v^-)/2$, respectively.

On the other hand, as in the one dimensional situation, the derivatives $\phi'_x, \phi''_x, \phi'''_x$ at (x_i, y_j) and $(x_{i+1/2}, y_j)$ and $\phi'_y, \phi''_y, \phi'''_y$ at (x_i, y_j) and $(x_i, y_{j+1/2})$ etc., can be approximated by simple central differences of suitable orders of accuracy described in previous subsection, again in a dimension by dimension fashion. The ϕ'_x at $(x_i, y_{j+1/2})$ is approximated by $((u')_{i,j+1/2}^+ + (u')_{i,j+1/2}^-)/2$, where $(u')_{i,j+1/2}^+$ is computed by (2.30) with ϕ, \bar{u} and \bar{v} replaced by ϕ', \bar{u}' and \bar{v}' , respectively. The computation of $(u')_{i,j+1/2}^+$ is mirror symmetric of that for $(u')_{i,j+1/2}^-$ with respect to $y_{j+1/2}$, and computation for $(v')_{i+1/2,j}^\pm$ is the same as that for $(u')_{i,j+1/2}^\pm$ with i and j interchanged. The ϕ''_x and ϕ'''_x at $(x_i, y_{j+1/2})$ are approximated by

$$\begin{aligned} (\phi''_x)_{i,j+1/2} &= \frac{1}{48} \left\{ \frac{1}{\Delta x} [4(\phi''_{i+1,j} - \phi''_{i-1,j} + \phi''_{i+1,j+1} - \phi''_{i-1,j+1})] \right. \\ &\quad + 2(-\bar{u}''_{i-1,j} - \bar{u}''_{i-1,j+1} + 10\bar{u}''_{i,j} + 10\bar{u}''_{i,j+1} - \bar{u}''_{i+1,j} - \bar{u}''_{i+1,j+1}) \\ &\quad \left. + 3(\bar{v}''_{i+1,j} - \bar{v}''_{i-1,j} - \bar{v}''_{i+1,j+1} + \bar{v}''_{i-1,j+1}) \right\}, \end{aligned} \quad (2.31)$$

and

$$\begin{aligned} (\phi'''_x)_{i,j+1/2} &= \frac{1}{48} \left\{ \frac{1}{\Delta x} [4(\phi'''_{i+1,j} - \phi'''_{i-1,j} + \phi'''_{i+1,j+1} - \phi'''_{i-1,j+1})] \right. \\ &\quad + 2(-\bar{u}'''_{i-1,j} - \bar{u}'''_{i-1,j+1} + 10\bar{u}'''_{i,j} + 10\bar{u}'''_{i,j+1} - \bar{u}'''_{i+1,j} - \bar{u}'''_{i+1,j+1}) \\ &\quad \left. + 3(\bar{v}'''_{i+1,j} - \bar{v}'''_{i-1,j} - \bar{v}'''_{i+1,j+1} + \bar{v}'''_{i-1,j+1}) \right\}, \end{aligned} \quad (2.32)$$

respectively. Similarly, ϕ''_y and ϕ'''_y at $(x_{i+1/2}, y_j)$ are approximated by (2.31) and (2.32) with i and j interchanged, respectively. Finally, the approximation of ϕ'' , ϕ''' , $\phi^{(4)}$ are obtained from (2.24)-(2.26) respectively.

3. Numerical Results

In this section we present the results of our numerical experiments for the fifth order HWENO schemes for one-dimensional and two-dimensional examples with the fourth order

Table 3.1: CPU time (in seconds) for the HWENO-LW and HWENO-RK schemes. Total CPU time for $N=10, 20, 40, 80, 160$ and 320 cells is recorded

	Example 3.1	Example 3.2	Example 3.3
HWENO-LW	0.53125	0.0625	36.75
HWENO-RK	1.484375	0.1875	115.703125

Table 3.2: $\phi_t + \phi_x = 0$. $\phi(x, 0) = \sin(\pi x)$. HWENO-LW and HWENO-RK schemes with periodic boundary conditions. $t = 2$. L_1 and L_∞ errors and numerical orders of accuracy. Uniform meshes with N cells

N	HWENO-LW				HWENO-RK			
	L_1 error	order	L_∞ error	order	L_1 error	order	L_∞ error	order
10	3.22E-02		4.50E-02		2.51E-02		3.49E-02	
20	1.42E-03	4.50	2.09E-03	4.43	1.13E-03	4.47	1.78E-03	4.29
40	5.04E-05	4.82	7.97E-05	4.71	4.46E-05	4.67	7.23E-05	4.62
80	1.63E-06	4.95	2.59E-06	4.94	1.54E-06	4.86	2.48E-06	4.87
160	3.73E-08	5.45	6.09E-08	5.41	3.62E-08	5.41	5.95E-08	5.38
320	3.22E-10	6.86	5.31E-10	6.84	3.18E-10	6.83	5.26E-10	6.82

Lax-Wendroff time discretization. A uniform mesh is used for all the test cases. The CFL number is taken as 0.6 for all test cases except for some accuracy tests where a suitably reduced time step is used to guarantee that spatial error dominates. The original HWENO scheme with the fourth order Runge-Kutta time discretization method for HJ equations by Qiu and Shu [19] with the same Lax-Friedrichs flux is used for comparison.

We first remark on the important issue of CPU timing and relevant efficiency of HWENO-LW schemes compared with HWENO-RK schemes. In general, the HWENO-LW schemes have smaller CPU cost for the same mesh and same order of accuracy in our implementation. For example, in Table 3.1, we provide a CPU time comparison between HWENO-LW and HWENO-RK schemes for accuracy tests in Examples 3.1, 3.2 and 3.3. We can see that the CPU cost for the HWENO-LW schemes is about one third of that for the HWENO-RK schemes. The computations are performed on a Dell OptiPlex(TM) GX620nSF, P4-3.2 with 1GB ram.

3.1. Accuracy tests

We first test the accuracy of the schemes on linear and nonlinear problems.

Example 3.1. We solve the following linear equation

$$\phi_t + \phi_x = 0 \quad (3.1)$$

with the initial condition $\phi(x, 0) = \sin(\pi x)$, and a 2-periodic boundary condition. We compute the solution up to $t = 2$, i.e. after one period by the HWENO-LW scheme and the HWENO-RK scheme. The numerical results are shown in Table 3.2. We can see that both schemes achieve their designed order of accuracy with comparable errors for the same mesh.

Example 3.2. We solve the following nonlinear scalar Burgers' equation

$$\phi_t + \frac{(\phi_x + 1)^2}{2} = 0 \quad (3.2)$$

with the initial condition $\phi(x, 0) = -\cos(\pi x)$, and a 2-periodic boundary condition. When $t = 0.5/\pi^2$ the derivative of solution is still smooth. The errors and numerical orders of accuracy

Table 3.3: Burgers' equation $\phi_t + (\phi_x + 1)^2/2 = 0$ with initial condition $\phi(x, 0) = -\cos(\pi x)$ by HWENO-LW and HWENO-RK schemes with periodic boundary conditions. $t = 0.5/\pi^2$. L_1 and L_∞ errors and numerical orders of accuracy. Uniform meshes with N cells

N	HWENO-LW				HWENO-RK			
	L_1 error	order	L_∞ error	order	L_1 error	order	L_∞ error	order
10	1.49E-03		5.53E-03		1.66E-03		7.80E-03	
20	9.31E-05	4.00	7.22E-04	2.94	1.04E-04	4.00	9.02E-04	3.11
40	4.48E-06	4.38	4.53E-05	3.99	4.59E-06	4.50	5.25E-05	4.10
80	1.63E-07	4.78	2.10E-06	4.43	1.65E-07	4.80	2.25E-06	4.54
160	4.02E-09	5.34	7.08E-08	4.89	4.08E-09	5.34	7.32E-08	4.94
320	8.25E-11	5.61	1.38E-09	5.68	8.31E-11	5.62	1.41E-09	5.70

Table 3.4: Two-dimensional Burgers' equation $\phi_t + (\phi_x + \phi_y + 1)^2/2 = 0$ with the initial condition $\phi(x, y, 0) = -\cos(\pi(x + y)/2)$ by HWENO-LW and HWENO-RK schemes with periodic boundary conditions. $t = 0.5/\pi^2$. L_1 and L_∞ errors and numerical orders of accuracy. Uniform meshes with $N_x \times N_y$ cells

$N_x \times N_y$	HWENO-LW				HWENO-RK			
	L_1 error	order	L_∞ error	order	L_1 error	order	L_∞ error	order
10×10	1.74E-03		5.78E-03		2.99E-03		8.96E-03	
20×20	9.82E-05	4.15	4.44E-04	3.70	1.07E-04	4.81	7.63E-04	3.55
40×40	4.42E-06	4.47	3.90E-05	3.51	4.73E-06	4.50	5.72E-05	3.74
80×80	1.58E-07	4.80	1.84E-06	4.41	1.65E-07	4.84	2.33E-06	4.62
160×160	4.41E-09	5.17	6.30E-08	4.87	5.93E-09	4.80	7.61E-08	4.94
320×320	1.01E-10	5.46	1.22E-09	5.69	1.62E-10	5.19	1.60E-09	5.57

by the HWENO-LW scheme and the HWENO-RK scheme are shown in Table 3.3. We also can see that both schemes achieve their designed order of accuracy. In fact, the HWENO-LW scheme has smaller errors than the HWENO-RK schemes for all meshes.

Example 3.3. We solve the following nonlinear scalar two-dimensional Burgers' equation

$$\phi_t + \frac{(\phi_x + \phi_y + 1)^2}{2} = 0, \quad (3.3)$$

with the initial condition $\phi(x, y, 0) = -\cos(\pi(x + y)/2)$, and a 4-periodic boundary condition. When $t = 0.5/\pi^2$ the solution is still smooth. The errors and numerical orders of accuracy by the HWENO-LW scheme and the HWENO-RK scheme are shown in Table 3.4. We also can see that both schemes achieve their designed order of accuracy, and the HWENO-LW scheme has smaller errors than the HWENO-RK scheme for the same mesh.

3.2. Test cases with discontinuous derivatives

Example 3.4. We solve the same nonlinear Burgers' equation (3.2) as in Example 3.2 with the same initial condition $\phi(x, 0) = -\cos(\pi x)$, except that we now plot the results at $t = 3.5/\pi^2$ when discontinuous derivative has already appeared in the solution. In Figure 3.1, the solutions of the HWENO-LW scheme and the HWENO-RK scheme with $N = 40$ and $N = 80$ cells are shown. We can see that both schemes give good results for this problem.

Example 3.5. We solve the nonlinear equation with a non-convex flux:

$$\phi_t - \cos(\phi_x + 1) = 0 \quad (3.4)$$

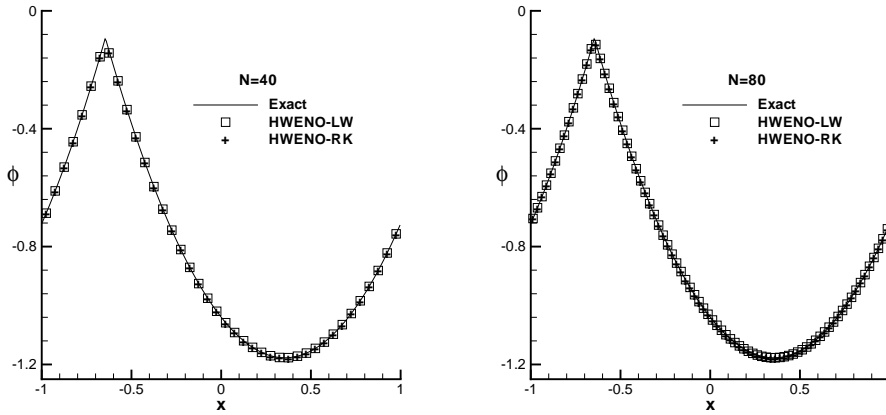


Fig. 3.1. Burgers' equation. $t = 3.5/\pi^2$. Left: $N = 40$. Right: $N = 80$. Solid lines: the exact solution; Square symbols: the HWENO-LW scheme; Plus symbols: the HWENO-RK scheme

with the initial data $\phi(x, 0) = -\cos(\pi x)$ and periodic boundary conditions. We plot the results at $t = 1.5/\pi^2$ when the discontinuous derivative has already appeared in the solution. In Figure 3.2, the solutions of the HWENO-LW scheme and the HWENO-RK scheme with $N = 40$ and $N = 80$ cells are shown. We also can see that both schemes give good results for this problem.

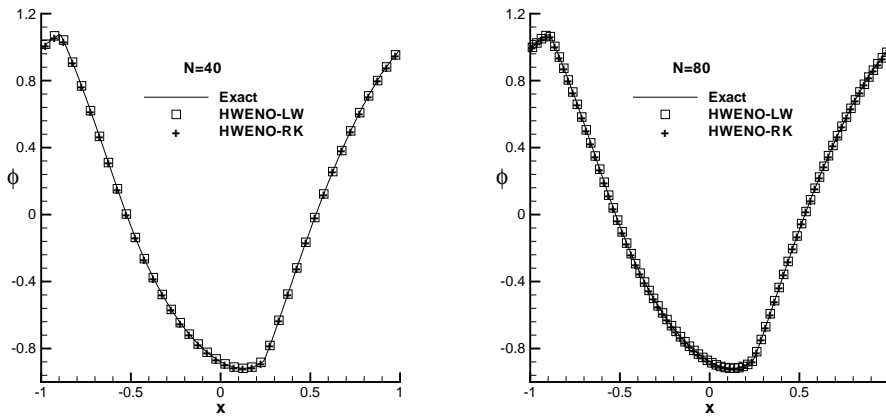


Fig. 3.2. Problem with the non-convex flux $H(u) = -\cos(u + 1)$. $t = 1.5/\pi^2$. Left: $N = 40$. Right: $N = 80$. Solid lines: the exact solution; Square symbols: the HWENO-LW scheme; Plus symbols: the HWENO-RK scheme

Example 3.6. We solve the one-dimensional Riemann problem with a non-convex flux:

$$\begin{cases} \phi_t - \frac{1}{4}(\phi_x^2 - 1)(\phi_x^2 - 4) = 0, & -1 < x < 1, \\ \phi(x, 0) = -2|x|. \end{cases} \quad (3.5)$$

This is a demanding test case, for many schemes have poor resolutions or could even converge to a non-viscosity solution for this case. We plot the results at $t = 1$ by the HWENO-LW scheme and the HWENO-RK scheme with $N = 40$ and $N = 80$ cells in Figure 3.3. We also can see

that both schemes give good results for this problem again.

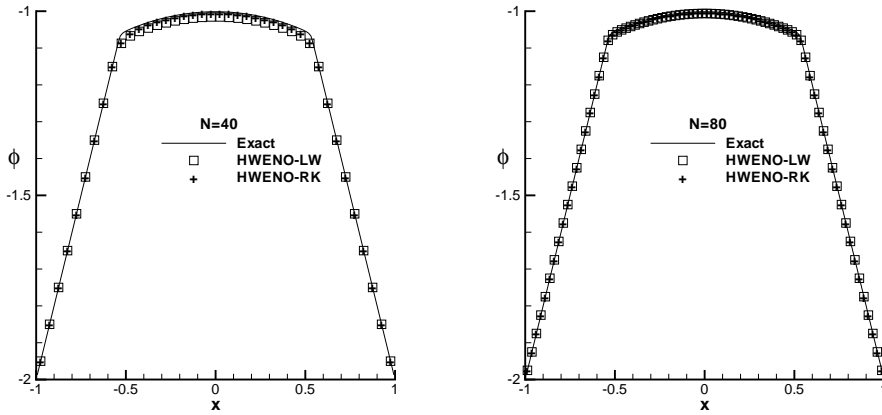


Fig. 3.3. Problem with the non-convex flux $H(u) = \frac{1}{4}(u^2-1)(u^2-4)$. $t = 1$. Left: $N = 40$. Right: $N = 80$. Solid lines: the exact solution; Square symbols: the HWENO-LW scheme; Plus symbols: the HWENO-RK scheme

Example 3.7. We solve the same two-dimensional nonlinear Burgers' equation (3.3) as in Example 3.3 with the same initial condition $\phi(x, 0) = -\cos(\pi(x + y)/2)$, except that we now plot the results at $t = 1.5/\pi^2$ when the discontinuous derivative has already appeared in the solution. The solution of the HWENO-LW scheme with $N_x \times N_y = 40 \times 40$ cells are shown in Figure 3.4. We observe good resolution for this example.

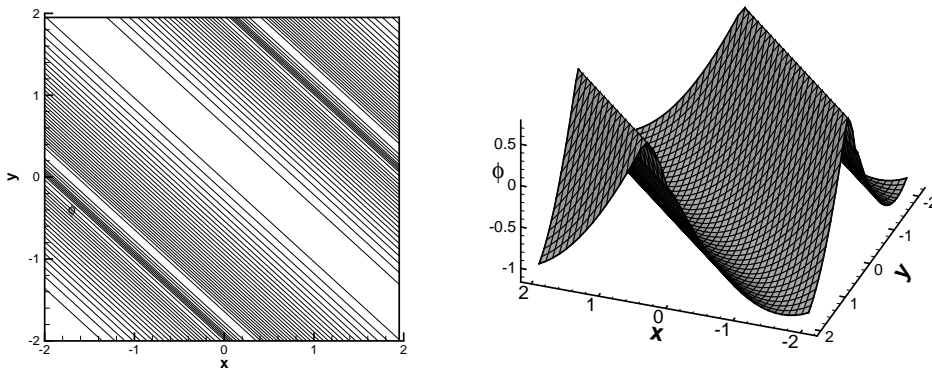


Fig. 3.4. Two-dimensional Burgers' equation. $t = 1.5/\pi^2$ by the HWENO-LW scheme with $N_x \times N_y = 40 \times 40$ cells. Left: contours of the solution. Right: surface of the solution

Example 3.8. The two-dimensional Riemann problem with a non-convex flux:

$$\begin{cases} \phi_t + \sin(\phi_x + \phi_y) = 0, & -1 < x, y < 1, \\ \phi(x, y, 0) = \pi(|y| - |x|). \end{cases} \quad (3.6)$$

The solution of the WENO-LW scheme with $N_x \times N_y = 40 \times 40$ cells are shown in Figure 3.5. We observe good resolution for this example.

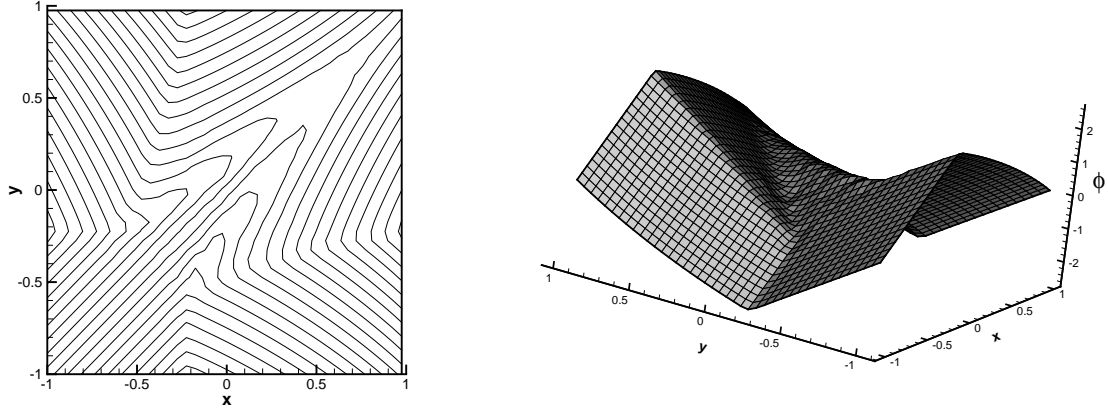


Fig. 3.5. Two-dimensional Riemann problem with a non-convex flux $H(u, v) = \sin(u + v)$, $t = 1$ by the HWENO-LW scheme with $N_x \times N_y = 40 \times 40$ cells. Left: contours of the solution. Right: surface of the solution

Example 3.9. A problem from optimal control is defined in $-\pi < x, y < \pi$

$$\begin{cases} \phi_t + \sin(y)\phi_x + (\sin x + \text{sign}(\phi_y))\phi_y - \frac{1}{2} \sin^2 y - (1 - \cos x) = 0, \\ \phi(x, y, 0) = 0, \end{cases} \quad (3.7)$$

with periodic conditions, see [14]. The solution of the HWENO-LW scheme with $N_x \times N_y = 60 \times 60$ cells and the optimal control $\omega = \text{sign}(\phi_y)$ are shown in Figure 3.6.

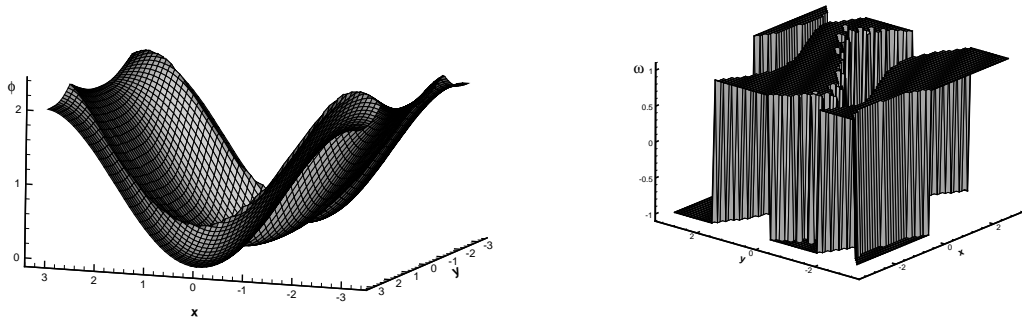


Fig. 3.6. The optimal control problem. $t = 1$ by the HWENO-LW scheme with $N_x \times N_y = 60 \times 60$ cells. Left: surfaces of the solution. Right: the optimal control $\omega = \text{sign}(\phi_y)$

Example 3.10. A two-dimensional eikonal equation with a non-convex Hamiltonian, which arises in geometric optics [7], is given by

$$\begin{cases} \phi_t + \sqrt{\phi_x^2 + \phi_y^2} + 1 = 0, & 0 \leq x, y < 1, \\ \phi(x, y, 0) = \frac{1}{4}(\cos(2\pi x) - 1)(\cos(2\pi y) - 1) - 1. \end{cases} \quad (3.8)$$

The solutions of the HWENO-LW scheme with $N_x \times N_y = 80 \times 80$ cells is shown in Figure 3.7. Good resolution is observed.

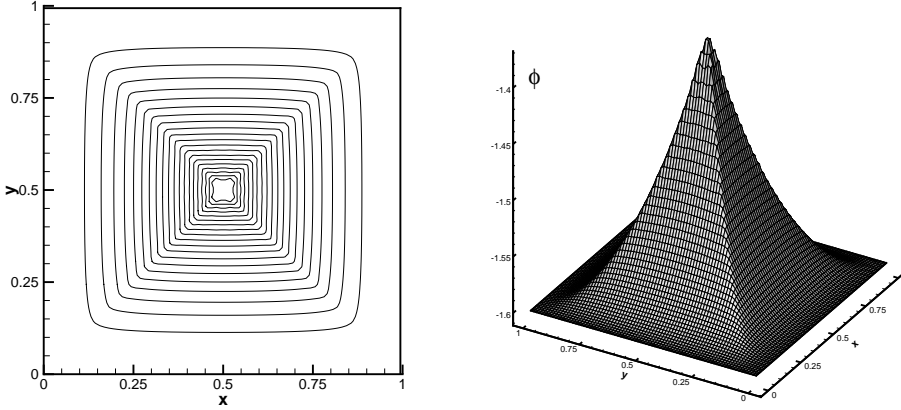


Fig. 3.7. Eikonal equation with a non-convex Hamiltonian. $t = 1$ by the HWENO-LW scheme with $N_x \times N_y = 80 \times 80$ cells. Left: contours of the solution. Right: surface of the solution

Example 3.11. The problem of a propagating surface [13] is governed by

$$\begin{cases} \phi_t - (1 - \varepsilon K) \sqrt{\phi_x^2 + \phi_y^2 + 1} = 0, & 0 \leq x, y < 1, \\ \phi(x, y, 0) = 1 - \frac{1}{4}(\cos(2\pi x) - 1)(\cos(2\pi y) - 1), \end{cases} \quad (3.9)$$

where K is the mean curvature defined by

$$K = -\frac{\phi_{xx}(1 + \phi_y^2) - 2\phi_{xy}\phi_x\phi_y + \phi_{yy}(1 + \phi_x^2)}{(1 + \phi_x^2 + \phi_y^2)^{\frac{3}{2}}},$$

and ε is a small constant. A periodic boundary condition is used. The approximation of the second derivative terms $\phi_{xx}, \phi_{xy}, \phi_{yy}$ and the extra terms of time derivatives $\phi'_{xx}, \phi'_{xy}, \phi'_{yy}$, etc., are constructed by the methods similar to that of the first derivative terms, but we only use linear weights in the reconstruction. The results of $\varepsilon = 0$ (pure convection) and $\varepsilon = 0.1$ by the HWENO-LW scheme with $N_x \times N_y = 50 \times 50$ cells are presented in Figure 3.8. The surfaces at $t = 0$ for $\varepsilon = 0$ and for $\varepsilon = 0.1$, and at $t = 0.1$ for $\varepsilon = 0.1$, are shifted downward in order to show the detail of the solution at later time.

4. Concluding Remarks

In this paper, a class of Hermite weighted essentially non-oscillatory (HWENO) schemes with a Lax-Wendroff time discretization procedure, termed HWENO-LW schemes, for solving one and two-dimensional Hamilton-Jacobi equations has been constructed. This is an alternative method for time discretization to the popular TVD Runge-Kutta time discretizations. We explore the possibility in avoiding the nonlinear weights for part of the procedure, hence reducing the cost but still maintaining non-oscillatory properties for problems with strong discontinuous derivative. As a result, comparing with the original HWENO with Runge-Kutta time discretizations schemes (HWENO-RK) of Qiu and Shu [19] for Hamilton-Jacobi equations, the major advantages of HWENO-LW schemes are their saving of computational cost and their compactness in the reconstruction. HWENO-LW has smaller errors than or is comparable with that given by HWENO-RK at same meshes for all cases we have computed.

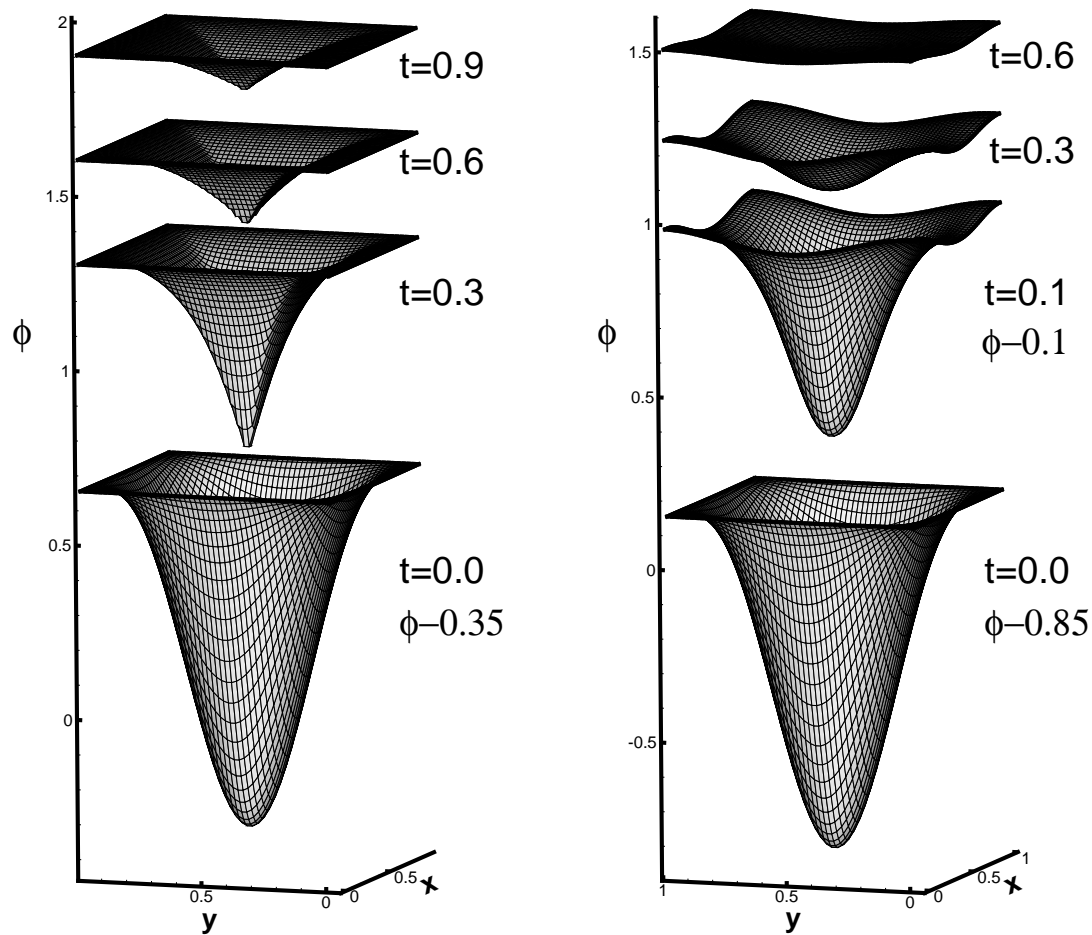


Fig. 3.8. Propagating surface. HWENO-LW scheme with $N_x \times N_y = 50 \times 50$ cells. Left: $\varepsilon = 0$; Right: $\varepsilon = 0.1$

References

- [1] S. Augoula and R. Abgrall, High order numerical discretization for Hamilton-Jacobi equations on triangular meshes, *J. Sci. Comput.*, **15** (2000), 198-229.
- [2] S. Bryson and D. Levy, High-order semi-discrete central-upwind schemes for multi-dimensional Hamilton-Jacobi equations, *J. Comput. Phys.*, **189** (2003), 63-87.
- [3] T.J. Barth and J.A. Sethian, Numerical schemes for the Hamilton-Jacobi and level set equations on triangulated domains, *J. Comput. Phys.*, **145** (1998), 1-40.
- [4] M. Dumbser and C.-D. Munz, Arbitrary high order discontinuous Galerkin schemes, in Numerical Methods for Hyperbolic and Kinetic Problems, S. Cordier, T. Goudon, E. Sonnendrcker (editors), EMS Publishing House, (2005), 295-333.
- [5] A. Harten, B. Engquist, S. Osher and S. Chakravathy, Uniformly high order accurate essentially non-oscillatory schemes, III, *J. Comput. Phys.*, **71** (1987), 231-303.
- [6] C. Hu and C.-W. Shu, A discontinuous Galerkin finite element method for Hamilton-Jacobi equations, *SIAM J. Sci. Comput.*, **21** (1999), 666-690.

- [7] S. Jin and Z. Xin, Numerical passage from systems of conservation laws to Hamilton-Jacobi equations, and relaxation schemes, *SIAM J. Numer. Anal.*, **35** (1998), 2163-2186.
- [8] G. Jiang and D. Peng, Weighted ENO schemes for Hamilton-Jacobi equations, *SIAM J. Sci. Comput.*, **21** (2000), 2126-2143.
- [9] G. Jiang and C.-W. Shu, Efficient implementation of weighted ENO schemes, *J. Comput. Phys.*, **126** (1996), 202-228.
- [10] A. Kurganov and E. Tadmor, New high-resolution semi-discrete central schemes for Hamilton-Jacobi equations, *J. Comput. Phys.*, **160** (2000), 720-742.
- [11] P.D. Lax and B. Wendroff, Systems of conservation laws, *Comm. Pure Appl. Math.*, **13** (1960), 217-237.
- [12] X. Liu, S. Osher and T. Chan, Weighted essentially non-oscillatory schemes, *J. Comput. Phys.*, **115** (1994), 200-212.
- [13] S. Osher and J. Sethian, Fronts propagating with curvature dependent speed: Algorithms based on Hamilton-Jacobi formulations, *J. Comput. Phys.*, **79** (1988), 12-49.
- [14] S. Osher and C.-W. Shu, High-order essentially nonoscillatory schemes for Hamilton-Jacobi equations, *SIAM J. Numer. Anal.*, **28** (1991), 907-922.
- [15] J. Qiu and C.-W. Shu, Finite difference WENO schemes with Lax-Wendroff-type time discretizations, *SIAM J. Sci. Comput.*, **24** (2003), 2185-2198.
- [16] J. Qiu, M. Dumbser and C.-W. Shu, The Discontinuous Galerkin Method with Lax-Wendroff Type Time Discretizations, *Computer Meth. Appl. Mech. Eng.*, **194** (2005), 4528-4543.
- [17] J. Qiu and C.-W. Shu, Hermite WENO schemes and their application as limiters for Runge-Kutta discontinuous Galerkin method: one dimensional case, *J. Comput. Phys.*, **193** (2004), 115-135.
- [18] J. Qiu and C.-W. Shu, Hermite WENO schemes and their application as limiters for Runge-Kutta discontinuous Galerkin method II: two dimensional case, *Computers and Fluids*, **34** (2005) 642-663.
- [19] J. Qiu and C.-W. Shu, Hermite WENO schemes for Hamilton-Jacobi equations, *J. Comput. Phys.*, **204** (2005), 82-99.
- [20] T. Schwartzkopff, C.D. Munz, and E.F. Toro, ADER: A high-order approach for linear hyperbolic systems in 2D, *J. Sci. Comput.*, **17** (2002), 231-240.
- [21] C.-W. Shu and S. Osher, Efficient implementation of essentially non-oscillatory shock capturing schemes II, *J. Comput. Phys.*, **83** (1989), 32-78.
- [22] V.A. Titarev and E.F. Toro, ADER schemes for three-dimensional nonlinear hyperbolic systems, *J. Comput. Phys.*, **204** (2005), 715-736.
- [23] Z. Xu and C.-W. Shu, Anti-diffusive finite difference WENO methods for shallow water with transport of pollutant, *J. Comput. Math.*, **24** (2006), 239-251.
- [24] Y.-T. Zhang and C.-W. Shu, High-order WENO schemes for Hamilton-Jacobi equations on triangular meshes, *SIAM J. Sci. Comput.*, **24** (2003), 1005-1030.